JBC RESEARCH ARTICLE

Upregulation of cholesterol synthesis by lysosomal defects requires a functional mitochondrial respiratory chain

Received for publication, March 14, 2024, and in revised form, April 27, 2024 Published, Papers in Press, May 21, 2024,
https://doi.org/10.1016/j.jbc.2024.107403

Francesco Agostini[1,‡], **Leonardo Pereyra**[2,‡], **Justin Dale**[1], **King Faisal Yambire**[3], **Silvia Maglioni**[4,5], **Alfonso Schiavi**[4], **Natascia Ventura**[4,5], **Ira Milosevic**[6,7], **and Nuno Raimundo**[1,8,*]

From the [1]*Department of Cellular and Molecular Physiology, Penn State College of Medicine, Hershey, Pennsylvania, USA;* [2]*Department of Cellular Biochemistry, University Medical Center, Goettingen, Germany;* [3]*Laboratory of Systems Cancer Biology, The Rockefeller University, New York, New York, USA;* [4]*IUF-Leibniz Research Institute for Environmental Medicine, Duesseldorf, Germany;* [5]*Institute for Clinical Chemistry and Laboratory Diagnostic, Medical Faculty, Heinrich Heine University, Duesseldorf, Germany;* [6]*Centre for Human Genetics, Nuffield Department of Medicine, University of Oxford, Oxford, UK;* [7]*Multidisciplinary Institute for Ageing, University of Coimbra, Coimbra, Portugal;* [8]*Penn State Cancer Institute, Penn State College of Medicine, Hershey, Pennsylvania, USA*

Reviewed by members of the JBC Editorial Board. Edited by George M. Carman

Mitochondria and lysosomes are two organelles that carry out both signaling and metabolic roles in cells. Recent evidence has shown that mitochondria and lysosomes are dependent on one another, as primary defects in one cause secondary defects in the other. Although there are functional impairments in both cases, the signaling consequences of primary mitochondrial dysfunction and lysosomal defects are dissimilar. Here, we used RNA sequencing to obtain transcriptomes from cells with primary mitochondrial or lysosomal defects to identify the global cellular consequences associated with mitochondrial or lysosomal dysfunction. We used these data to determine the pathways affected by defects in both organelles, which revealed a prominent role for the cholesterol synthesis pathway. We observed a transcriptional upregulation of this pathway in cellular and murine models of lysosomal defects, while it is transcriptionally downregulated in cellular and murine models of mitochondrial defects. We identified a role for the post-transcriptional regulation of transcription factor SREBF1, a master regulator of cholesterol and lipid biosynthesis, in models of mitochondrial respiratory chain deficiency. Furthermore, we found that retention of Ca^{2+} in lysosomes of cells with mitochondrial respiratory chain defects contributes to the differential regulation of the cholesterol synthesis pathway in the mitochondrial and lysosomal defects tested. Finally, we verified *in vivo*, using a model of mitochondria-associated disease in *Caenorhabditis elegans* that normalization of lysosomal Ca^{2+} levels results in partial rescue of the developmental delay induced by the respiratory chain deficiency.

Mitochondria and lysosomes are two fundamental organelles for metabolism. Mitochondria carry out the bulk of aerobic metabolism and have fundamental roles in Fe-S cluster synthesis, while lysosomes harbor the machinery to degrade macromolecules, obtained from intracellular and extracellular environments, and return the building blocks to the cytoplasm and other organelles for biosynthetic reactions.

In addition to their long-established metabolic functions, both of these organelles play important roles as signaling platforms, which remain an active area of investigation. Multiple signaling pathways have been implicated in response to perturbations in mitochondrial function and dynamics, some of these acting in a tissue-specific manner (1). The mitochondrial unfolded protein response seems to integrate several aspects of the cellular response to mitochondrial stress in different tissues (2). However, some perturbations in mitochondrial function also affect the activity of the metabolic signaling hub AMP-activated protein kinase (AMPK), depending on the specific mitochondrial defect and the tissue affected (3–7). AMPK and another signaling hub, mechanistic target of rapamycin complex 1 (mTORC1), function as respective coordinators of catabolism and anabolism (8, 9); mTORC1 promotes cellular anabolism, while AMPK represses anabolic pathways and stimulates catabolism (10, 11). mTORC1 signaling is also impacted in some instances of mitochondrial malfunction, in a defect- and tissue-specific manner (12–14). Notably, both mTORC1 and AMPK can be recruited to the lysosomal membrane for activation, thus highlighting the importance of mitochondria-lysosome coordination in the regulation of cellular metabolism (15).

Perturbations of lysosomal function have also been shown to affect the cellular signaling hub mTORC1 (16, 17). Further, acidification of the lysosomal lumen is needed for the activity of the hydrolases and for cholesterol efflux from lysosomes to endoplasmic reticulum (ER) (18, 19). Loss of lysosomal acidification results in functional iron deficiency and pseudohypoxia signaling (20–22).

Importantly, mitochondria and lysosomes are interdependent (23, 24). Impairment of the mitochondrial respiratory chain (RC) and/or mitochondrial dynamics results in dysfunctional lysosomes with excessive storage of undigested material in the lysosomal lumen (7, 25, 26). Lysosomal defects in sphingolipid

‡ These authors contributed equally to this work.
* For correspondence: Nuno Raimundo, nuno.raimundo@psu.edu.

catabolism, cholesterol trafficking, and impaired lysosomal acidification result in repression of the transcriptional program of mitochondrial biogenesis and impaired RC function (27). The mitochondrial unfolded protein response signaling in response to mitochondrial malfunction is partially mediated by lysosomes (28, 29). Furthermore, mitochondria and lysosomes physically interact with each other *via* membrane contact sites, as well as with other organelles, especially the ER (30, 31). The contact sites between mitochondria and lysosomes have been linked to the ability of lysosomes to regulate mitochondrial dynamics by stimulating mitochondrial fission (32).

While there is a negative feedback between mitochondrial and lysosomal malfunction, it is still not clear how defective mitochondria and lysosomes impact other cellular processes, in particular lipid homeostasis. Here, we use bulk cellular transcriptome data to unveil the signaling pathways that are affected by mitochondrial and lysosomal malfunction. We show that these two organelles have opposite impacts on the synthesis of lipids, particularly on SREBF1-dependent cholesterol synthesis, and that these effects are independent of AMPK and mTORC1 signaling. These results contribute to our understanding of the complexity of organelle cross talk and its interplay with cellular metabolism.

Results

Mitochondria and lysosomal defects have opposite effects on regulation of cholesterol synthesis

Mitochondria and lysosomes show functional interdependence: the dysfunction of one leads to dysfunction in the other. As both organelles have signaling roles, we sought to determine which aspects of cellular signaling and metabolism are affected by both mitochondria and lysosomal dysfunction. To study the signaling environment in a broad and unbiased manner, we characterized the cellular transcriptome using bulk RNA sequencing. To model organelle dysfunction, we used several human and murine cellular models of chronic mitochondrial and lysosomal malfunction (see Fig. 1*A*). To model mitochondrial malfunction, we used complex III deficiency, achieved through the stable knock down of complex III subunit UQCRC1, through lentivirus-delivered shRNA in HeLa cells. This model will henceforth be referred to as UQCRC1-kd (7). We have previously shown that these cells are an adequate model of mitochondrial RC deficiency, with decreased O_2 consumption and increased superoxide levels (7).To model lysosomal malfunction, we used HeLa cells with a stable shRNA-mediated silencing of acid alpha-glucosidase (GAA-kd) or of cathepsin B (CTSB-kd) (Fig. S1). GAA is the enzyme responsible for the hydrolysis of glycogen to glucose in the lysosomal lumen, and CTSB is a member of the calpain-like family of cysteine lysosomal proteases. Both GAA and CTSB are located at the lysosomal lumen.

For each gene silenced, we used two clones of HeLa cells, each made with a different shRNA, and two clones with scrambled shRNA as controls. First, we identified the differentially expressed transcripts between the two UQCRC1-kd lines and the control lines, and those differentially expressed between the lysosomal lines and the controls. For the mitochondrial defects, we obtained 2116 differentially expressed genes (DEG) between UQCRC1-kd and scrambled control, of which 501 were upregulated in UQCRC1-kd and 1615 downregulated (Fig. 1*B*). The lysosomal defects models yielded 2877 DEG, of which 994 were upregulated (comparing all lines of GAA-kd and CTSB-kd *versus* the two controls) and 1883 downregulated (Fig. 1*C*). The DEG lists are presented in Table S1.

Interestingly, when we subjected these DEG lists to pathway analysis using the Ingenuity Pathway (https://digitalinsights.qiagen.com/products-overview/discovery-insights-portfolio/analysis-and-visualization/qiagen-ipa/) analysis software (Qiagen), the most enriched pathways in both the mitochondrial and lysosomal defects were all related with the synthesis of mevalonate and cholesterol (Fig. 1, *D* and *E*). Yet, while the transcript levels of cholesterol synthesis enzymes were globally upregulated in the lysosomal defects, they were globally downregulated in the mitochondrial defects (Fig. 1*F*).

To confirm this observation, we isolated RNA from a different batch of UQCRC1-kd and control cells, and measured the transcript levels of cholesterol synthesis enzymes by quantitative real-time PCR (qPCR). In agreement with the RNAseq results, we observed that the transcript levels of cholesterol synthesis enzymes are globally downregulated in UQCRC1-kd cells (Fig. 2*A*). To test if different perturbations of the RC would have the same impact on cholesterol synthesis, we used embryonic fibroblasts isolated from mice lacking a subunit of complex I, NDUFS4 (NDUFS4-KO) and the corresponding WT littermate controls. In these murine cells, similarly to the human cells, the transcript levels of cholesterol synthesis enzymes were also downregulated (Fig. 2*B*), supporting a transcriptional downregulation of this pathway in response to RC impairments.

Next, we examined if our findings in cultured cells were also valid *in vivo*. We used the livers of NDUFS4-KO mice and their WT littermates and observed that the transcript levels of cholesterol synthesis enzymes were globally decreased in NDUFS4-KO livers (Fig. 2*C*). Similar results were obtained in brains isolated from NDUFS4-KO mice (Fig. 2*D*). Altogether, these results show that chronic perturbations in mitochondrial RC lead to transcriptional downregulation of cholesterol synthesis enzymes, both in cultured cells and in multiple mouse organs.

Next, we sought to validate the transcriptome results obtained with cells harboring lysosomal defects. We tested new vials of HeLa GAA-kd and CTSB-kd, and again observed an upregulation of the transcript levels of cholesterol synthesis enzymes by qPCR (Fig. 3*A*). We also examined mouse fibroblasts lacking lysosomal proteins, namely GAA-KO (Fig. 3*B*), cathepsin L (CTSL)-KO (Fig. 3*C*), CTSB-KO (Fig. 3*D*), and LAMP2-KO (Fig. 3*E*). In all the cases, we observed a robust upregulation of the transcript levels of cholesterol synthesis enzymes, albeit to varying degrees of magnitude. To test if these results could also be observed *in vivo*, we measured the transcript levels of cholesterol synthesis enzymes in the liver of GAA-KO mice and observed an increase in the expression of at least two enzymes (Fig. 3*F*). These results show that

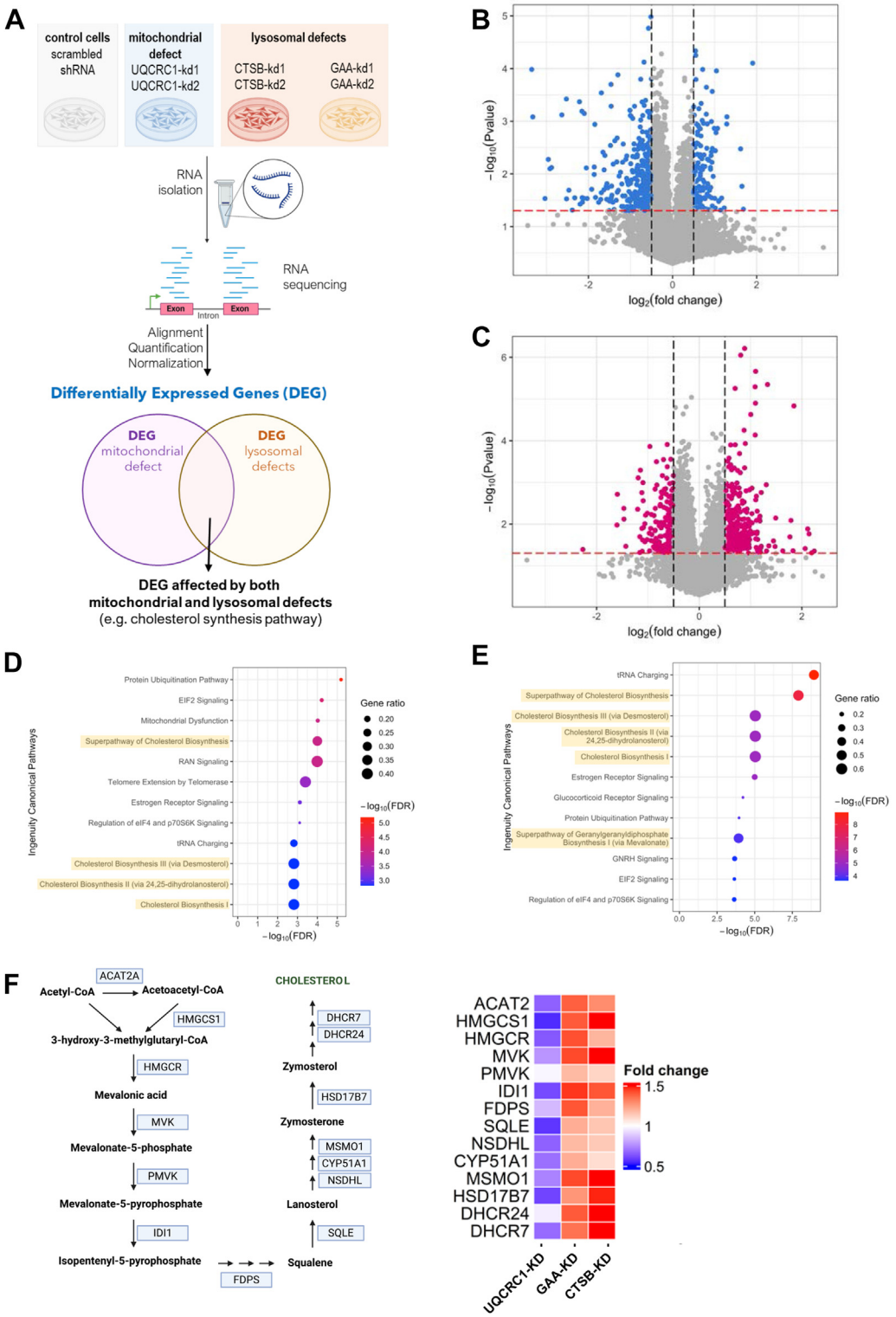

Figure 1. Defects in mitochondria and lysosomes have opposing effects on the regulation of cholesterol synthesis pathway. *A*, schematic representation of the RNAseq analysis workflow in which one mitochondrial (UQCRC1-kd) and two lysosomal (CTSB-kd and GAA-kd) dysfunction models were examined. *B* and *C*, volcano plots of the transcriptome data analyses showing the differentially expressed genes between UQCRC1-kd and control HeLa lines (*B*), and those differentially expressed between the CTSB-kd and GAA-kd lines and the controls (*C*). *D*, canonical pathways altered in the mitochondrial dysfunction cell model and (*E*) in the lysosomal defective cell models. The cholesterol biosynthesis super pathways are shadowed. Associated *p* values were determined according to the analysis in the database for annotation, visualization, and integrated discovery (Fisher exact *p*-value). *F*, (*Left*) representation of the cholesterol synthesis pathway. Genes coding the enzymes are indicated. (*Right*) heatmaps showing the respective transcripts levels (fold change) in UQCRC1-kd, GAA-kd, and CTSB-kd cells. CTSB, cathepsin B; GAA, acid alpha-glucosidase.

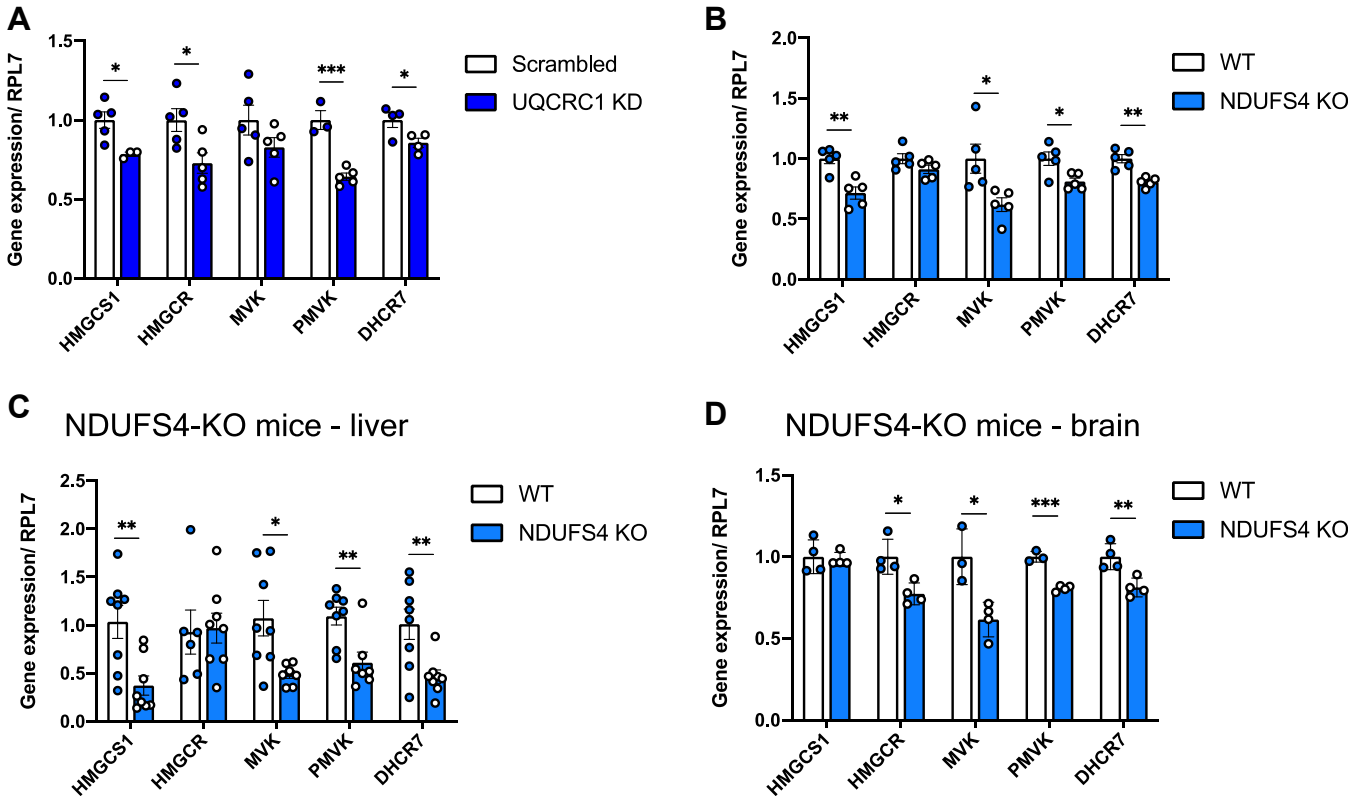

Figure 2. Expression of cholesterol synthesis enzymes is inhibited in cells and organs with mitochondrial respiratory chain deficiency. qPCR of genes involved in the cholesterol synthesis pathway was performed in control and UQCRC1-kd HeLa cells (*A*), NDUFS4 WT and KO MEF cells (*B*), and in the livers and brains of NDUFS4 WT and KO mice (*C* and *D*). At least four independent samples/animals were evaluated. Statistical significance between control and mutant samples for each gene was determined by unpaired *t* test, $*p < 0.05$, $**p < 0.01$, $***p < 0.001$. MEF, mouse embryonic fibroblast; qPCR, quantitative real-time PCR.

impairment of lysosomal function results in a transcriptional upregulation of cholesterol synthesis enzymes, both in cultured cells and *in vivo* organs. Of note, these results are consistent with the transcriptional upregulation of cholesterol synthesis upon treatment with an inhibitor of the lysosomal v-ATPase, bafilomycin A1 (20, 33, 34).

It is known that lysosomal cholesterol egress requires the joint action of the proteins NPC2 and NPC1, as well as acidic pH in the lysosomal lumen (34). While a subpopulation of lysosomes is unable to acidify properly in cells lacking GAA (20, 35), there is no indication that loss of CTSB or CTSL impairs lysosomal acidification, although these proteases may be involved in NPC1 maturation (36). Furthermore, in UQCRC1-kd cells, lysosomal pH is increased, there is lysosomal Ca^{2+} accumulation and inhibited lysosomal hydrolysis (7). This suggests that lysosomal impairment leads to increased expression of cholesterol synthesis enzymes but only when the mitochondrial RC is functional. We therefore sought to further explore the mechanisms underlying the differential regulation of cholesterol synthesis enzyme expression under mitochondrial and lysosomal defects.

Downregulation of cholesterol synthesis pathway in cells with mitochondrial malfunction is associated with decreased SREBF1 processing and activity

The synthesis of cholesterol is regulated at the transcript level by two transcription factors, SREBF1 and SREBF2 (37). These proteins are tethered to the ER membrane through interactions with SCAP (37), in a cholesterol-dependent manner: high levels of cholesterol in the ER membrane retain the SCAP/SREBF1 or SCAP/SREBF2 complexes at the ER, while a decrease in ER cholesterol content releases them for further activation (37). The retention of SCAP/SREBF1 or SCAP/SREBF2 complexes at the ER membrane is also stimulated by two proteins, INSIG1 and INSIG2. After their release from the ER, the proteins are further processed at the Golgi by two proteases S1P and S2P, and released in their mature form to translocate to the nucleus. Here, they bind the promoters of their target genes and stimulate transcription (37). Given that the effect of UQCRC1-kd and NDUFS4-KO on the transcriptional regulation of cholesterol synthesis is similar, we used the NDUFS4-KO cells to follow this up mechanistically. We observed that in NDUFS4-KO whole cell extracts, mature SREBF1 was decreased (Fig. 4*A*), while SREBF2 protein levels were similar in NDUFS4-KO and WT cells (Fig. 4*B*). The transcript levels of SREBF1 and SREBF2 were not changed in the NDUFS4-KO cells (Fig. S2*A*), suggesting that the reason underlying the decrease in SREBF1 protein levels is post-transcriptional. To further explore why SREBF1 levels are decreased in NDUFS4-KO cells, we briefly treated the cells with the proteasome inhibitor MG132 (2 h, 10 μM) to determine if ubiquitin-mediated proteasomal degradation may be responsible. SREBF1 can be degraded by the proteasome when it is phosphorylated at Ser73 by the kinase GSK-3B, which

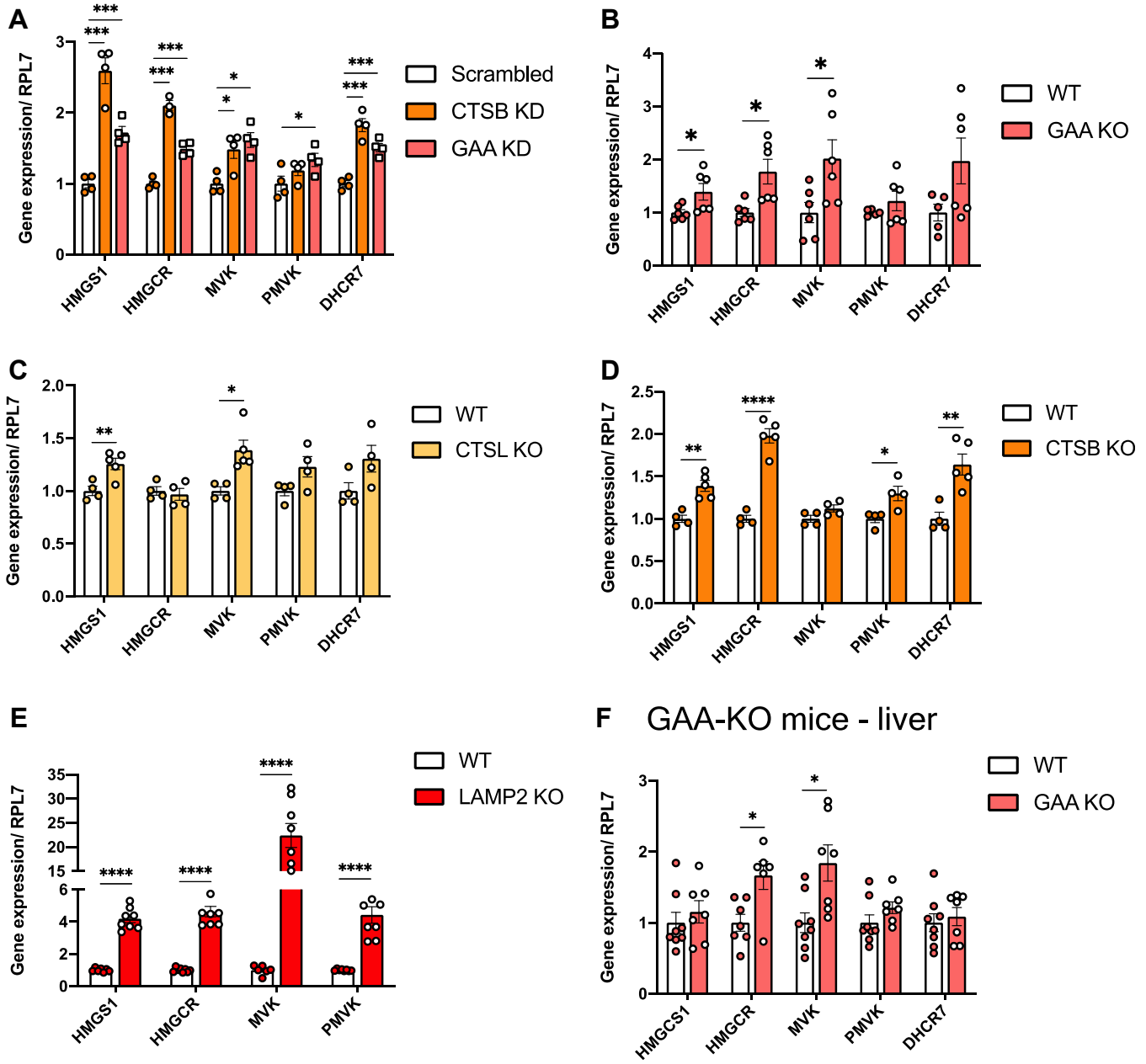

Figure 3. Transcriptional control of cholesterol synthesis is upregulated in cells and organs with lysosomal defects. *A*, qPCR showing the transcript level of cholesterol synthesis enzymes in CTSB-kd, GAA-kd, and control HeLa cells. At least three independent samples were evaluated. Statistical significance between control and mutant samples for each gene was determined by two-way ANOVA with Tukey's multiple comparisons test. *$p < 0.05$, **$p < 0.01$, ***$p < 0.001$. The same set of transcripts was analyzed *via* qPCR in KO MEFs for GAA (*B*), CTSL (*C*), CTSB (*D*), LAMP2 (*E*), and relative WT controls, as well as in the livers of GAA WT and KO mice (*F*). At least four independent animals were evaluated. Unpaired *t* test was used to determine the statistical significance between control and KO samples for each gene. *$p < 0.05$, **$p < 0.01$, ***$p < 0.001$, ****$p < 0.0001$. CTSB, cathepsin B; GAA, acid alpha-glucosidase; MEF, mouse embryonic fibroblast; qPCR, quantitative real-time PCR.

allows the ubiquitin ligase FBXW7 to recognize SREBF1 and ubiquitinate it (38). Curiously, in MG132-treated NDUFS4-KO cells, the levels of SREBF1 were returned to the levels present in WT cells (Fig. 4*A*), while no changes were observed in SREBF2 levels (Fig. 4*B*). These results suggest that in cells with RC deficiency, SREBF1 is continuously degraded, in a proteasome-dependent manner.

Our result also implies that GSK3B activity may be increased in response to RC impairment. Therefore, we probed the levels of GSK3B in NDUFS4-KO whole cell extracts (Fig. 4*C*) as well as the phosphorylation status of Ser9/21 (both inhibitory of GSK3B when phosphorylated). The ratio between GSK3B-Ser9/21-P and total GSK3B was decreased (Fig. 4*C*), which suggests that the activity of GSK-3B is increased in cells with impaired mitochondrial RC.

While the levels of SREBF1/2 immature precursors may impact their activity, the key regulatory step is maturation. Because the activity of mature SREBF1/2 is associated with its nuclear localization, we next prepared nuclear extracts from WT and NDUFS4-KO cells and observed a decrease in

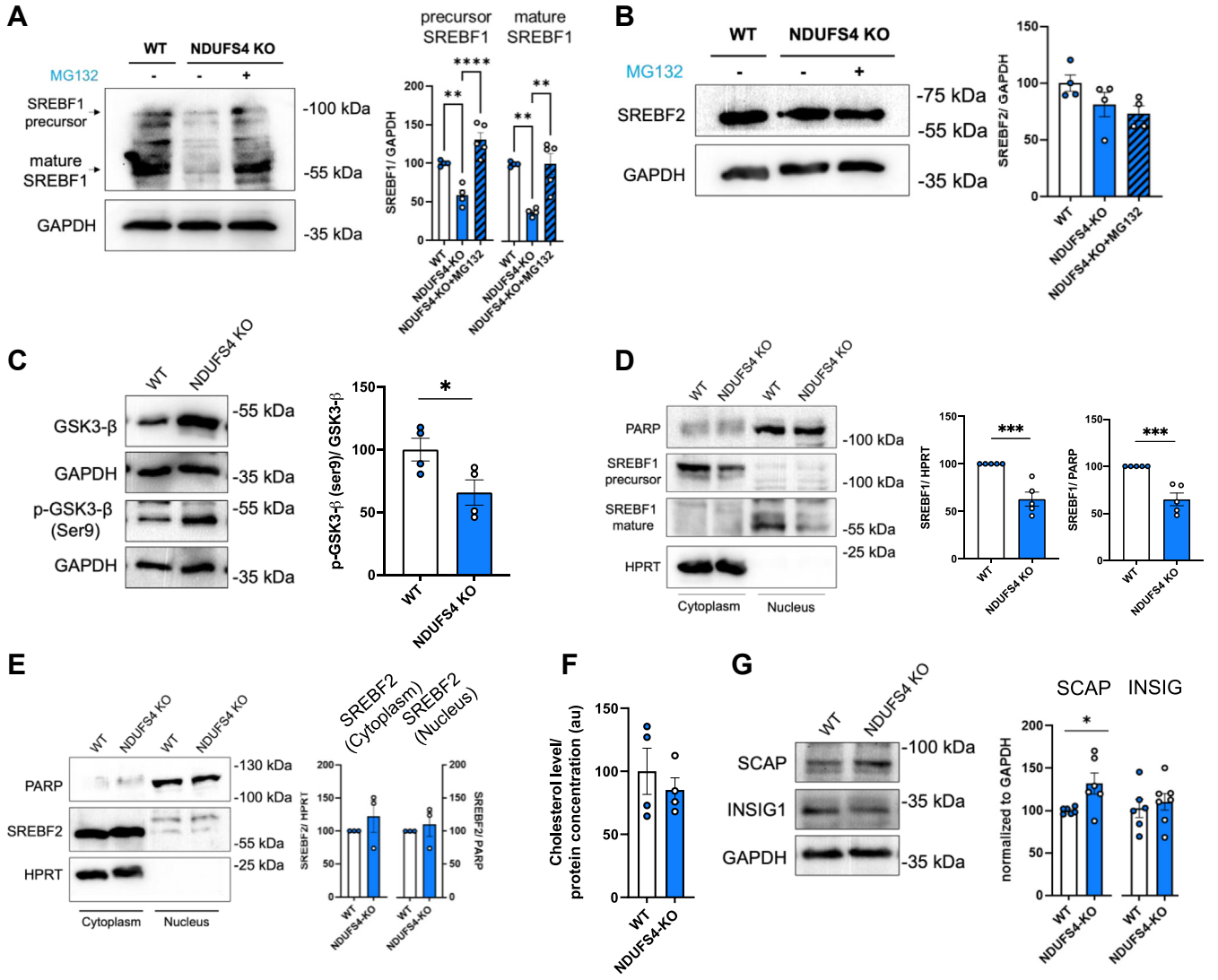

Figure 4. Mitochondrial defects impair the cholesterol pathway by altering SREBF1 processing and activity. *A* and *B*, Western blot analyses of SREBF1 (*A*) and SREBF2 (*B*) in WT and NDUFS4-KO fibroblasts, both untreated and treated with the proteasome inhibitor MG132 (2 h, 10 μM). GAPDH was used as the loading control. At least four independent experiments were evaluated. Statistics: one-way ANOVA with Tukey's multiple comparisons test, $*p < 0.05$, $**p < 0.01$, $****p < 0.0001$. *C*, Western blot analysis showing total GSK3B and its phosphorylation at Ser9. GAPDH was used as loading control. Four independent samples were evaluated and unpaired *t* test was used for statistical analysis. $***p < 0.001$, *D* and *E*, Western blots of nuclear *versus* cytosolic fractions from WT and NDUFS4-KO fibroblasts probed with anti-SREBF1 (*D*), anti-SREBF2 (*E*), anti-PARP (nuclear marker), and anti HPRT (cytosolic marker) antibodies. At least four independent experiments were done. Statistics: unpaired *t* test, $***p < 0.001$. *F*, cholesterol level measured in the ER fractions isolated from WT and NDUFS4-KO MEFs. The level of cholesterol was normalized by the total amount of protein in the corresponding fraction. Four independent samples were analyzed. No statistically significant difference was observed with an unpaired *t* test. *G*, Western blot analysis showing the level of SCAP and INSIG1 levels in WT and NDUFS4-KO fibroblasts. At least six independent samples were evaluated. Unpaired *t* test, $*p < 0.05$. ER, endoplasmic reticulum; HPRT, hypoxanthine-guanine phosphoribosyltransferase; MEF, mouse embryonic fibroblast.

SREBF1 levels in the nucleus of NDUFS4-KO fibroblasts (Fig. 4*D*), supporting the decreased activity of SREBP1 in these cells. We also observed that nuclear levels of SREBF2 in NDUFS4-KO cells were similar to WT (Fig. 4*E*). Further, the levels of mature SREBF1 were increased in cellular models of lysosomal defects, namely mouse fibroblasts lacking CTSB and CTSL (Fig. S2*B*).

As mentioned above, the levels of cholesterol in the ER membranes determine if SREBF1/2 remain sequestered by SCAP at the ER membrane or are released and further processed to promote its nuclear localization and transcriptional activity. This could be explained by perturbation of cholesterol levels in the ER of cells with mitochondrial defects (higher ER cholesterol levels) and lysosomal defects (lower ER cholesterol levels). We therefore tested if the levels of ER cholesterol were altered in cells with RC deficiency. Using a biochemical procedure, we isolated the ER (Fig. S2, *C* and *D*) and using the ER-rich fractions, we measured the levels of cholesterol. We observed no difference in the amount of cholesterol in ER membranes from WT and NDUFS4-KO cells (Fig. 4*F*), or in the total cellular cholesterol levels (Fig. S2*E*). Given that there are no changes in cholesterol concentration in the ER that can explain the lower levels of mature SREBF1 in NDUFS4-KO cells, we tested if the proteins that process the maturation of

SREBF1 might be affected in NDUFS4-KO cells. We observed that the protein levels of SCAP are increased in NDUFS4-KO cells relative to WT, while the levels of INSIG remain unchanged (Fig. 4*G*), implying that the decreased maturation of SREBF1 is not due to lower levels of its processing proteins.

Altogether, these results show that the levels of SREBF1 precursor protein, and consequently the activity of mature SREBF1, are decreased in the models of RC deficiency, while increased SREBF1 processing and activity occur in lysosomal malfunction models. Given that the cells with RC deficiency also have defective lysosomes, the inhibition of the RC seems to modify the effect of lysosomal malfunction on cholesterol homeostasis. This involves the GSK-3B-mediated degradation of SREBF1 in cells with mitochondrial RC impairments.

The mechanisms of cholesterol trafficking and homeostasis are fully functional in cells with mitochondrial malfunction

To test if other mechanisms besides SREBF1 regulation affect cholesterol homeostasis in cells with RC deficiency, we probed cholesterol trafficking. Cholesterol can reach the ER *via* lysosomes or *via* the plasma membrane (39). Egress of cholesterol from the lysosomal lumen and its trafficking to the ER is a key process affected by loss of lysosomal acidification or loss of the proteins NPC2 and NPC1. These factors are both necessary to harness cholesterol from the lysosomal lumen and transfer it to the ER membrane, respectively (40–42).

To test the hypothesis that cholesterol transfer from lysosomes to the ER was involved in the transcriptional repression of cholesterol synthesis enzymes in RC-deficient cells, we treated NDUFS4-KO and WT fibroblasts with the NPC1 inhibitor U18666A (10 μM, 4 h), thus blocking a key protein involved in the lysosome-ER cholesterol transfer. We observed that inhibition of NPC1 is sufficient to abolish the transcriptional repression of cholesterol synthesis enzymes in NDUFS4-KO cells (Fig. 5*A*). Notably, the treatment with U18666A resulted in similar induction of transcripts of cholesterol enzymes in NDUFS4-KO and WT cells (Fig. 5*A*).

The profound effect of the NPC1 inhibitor suggests that the transfer of cholesterol from lysosomes to the ER is undisturbed in NDUFS4-KO cells. Furthermore, inhibition of NPC1 results in decreased ER cholesterol, and therefore this result further demonstrates that the cholesterol homeostatic mechanisms in the ER are functional in these cells. To confirm this, we checked the protein levels of mature SREBF1, and observed that they were significantly increased, both in WT and NDUFS4-KO, upon NPC1 inhibition (Fig. 5*B*). It is noteworthy that the protein levels of NPC1 and NPC2, two key enzymes involved in lysosomal cholesterol efflux toward ER, are not changed in NDUFS4-KO cells compared to WT (Fig. S3*A*).

To further test that depletion of ER cholesterol levels could increase the expression of cholesterol synthesis enzymes in RC-deficient cells, we added 2-hydroxypropyl-beta-cyclodextrin (a cholesterol-depleting metabolite) to the WT and NDUFS4-KO cells. We observed that both WT and NDUFS4-KO show a robust increase in the transcript levels of cholesterol synthesis enzymes when cholesterol is depleted (Fig. S3*B*). Notably, this effect was also observed in cells with lysosomal defects (CTSB-KO and CTSL-KO), showing that these cells are also able to respond dynamically to changes in cholesterol levels (Fig. S3*C*).

Together, these results underscore that RC-deficient cells can dynamically respond to changes in ER cholesterol content. However, under basal conditions, these cells seem to exhibit increased cholesterol egress from the lysosomes to the ER, thus decreasing the activity of SREBF1 and the transcript levels of its target genes.

As shown above, the response of cholesterol homeostasis to lysosomal defects is modified in cells with impaired mitochondrial RC. To further test this premise using a pharmacological approach, we sought to inhibit the RC in cells with lysosomal defects, which have increased the expression of cholesterol synthesis enzymes. Thus, we treated HeLa CTSB-kd cells with the Rc complex I inhibitor rotenone (250 nM for 24 h). We observed a robust decrease of the transcript levels of cholesterol synthesis enzymes (Fig. 5*C*). This result supports the concept that transcriptional upregulation of cholesterol synthesis in response to lysosomal defects requires a functional RC.

The distribution of cholesterol through cellular membranes relies on organelle contact sites. In cells lacking NPC1, there are fewer contacts between lysosomes and ER, and thus less delivery of cholesterol from the lysosomes to the ER, which is a trigger for increased cholesterol synthesis (43). Therefore, we tested if the lysosome-ER contacts were affected in NDUFS4-KO cells. We used a proximity ligation assay (PLA) that emits a fluorescent signal when the antibodies against the lysosomal marker LAMP1 and the ER marker SERCA2A are closer than 40 nm, and therefore within the expected range of membrane contact sites (44). With this LAMP1-SERCA2A PLA, we observed an increase in lysosome-ER contacts in NDUFS4-KO cells (Fig. 5*D*). These results suggest that the increased association of lysosomes and ER in RC-deficient may contribute to enhanced lysosomal cholesterol delivery to the ER membrane leading to downregulation of cholesterol synthesis in RC-deficient cells.

The downregulation of cholesterol synthesis pathway in cells with mitochondrial malfunction is independent of AMPK signaling

AMPK responds to acute mitochondrial stresses and represses the activity of HMGCR (45). This repression modulates the metabolic flux through the cholesterol synthesis pathway. Therefore, we sought to test whether AMPK signaling was involved in the downregulation of cholesterol synthesis enzyme expression in RC-deficient cells. We already showed that the HeLa UQCRC1-kd cells have decreased AMPK signaling (7). Thus, we tested if manipulating AMPK activity would be sufficient to impact cholesterol synthesis in respiratory chain deficient cells. For that, we used mouse embryonic fibroblasts (MEFs) lacking both α1 and α2 AMPK catalytic subunits (AMPK double knockout, henceforth

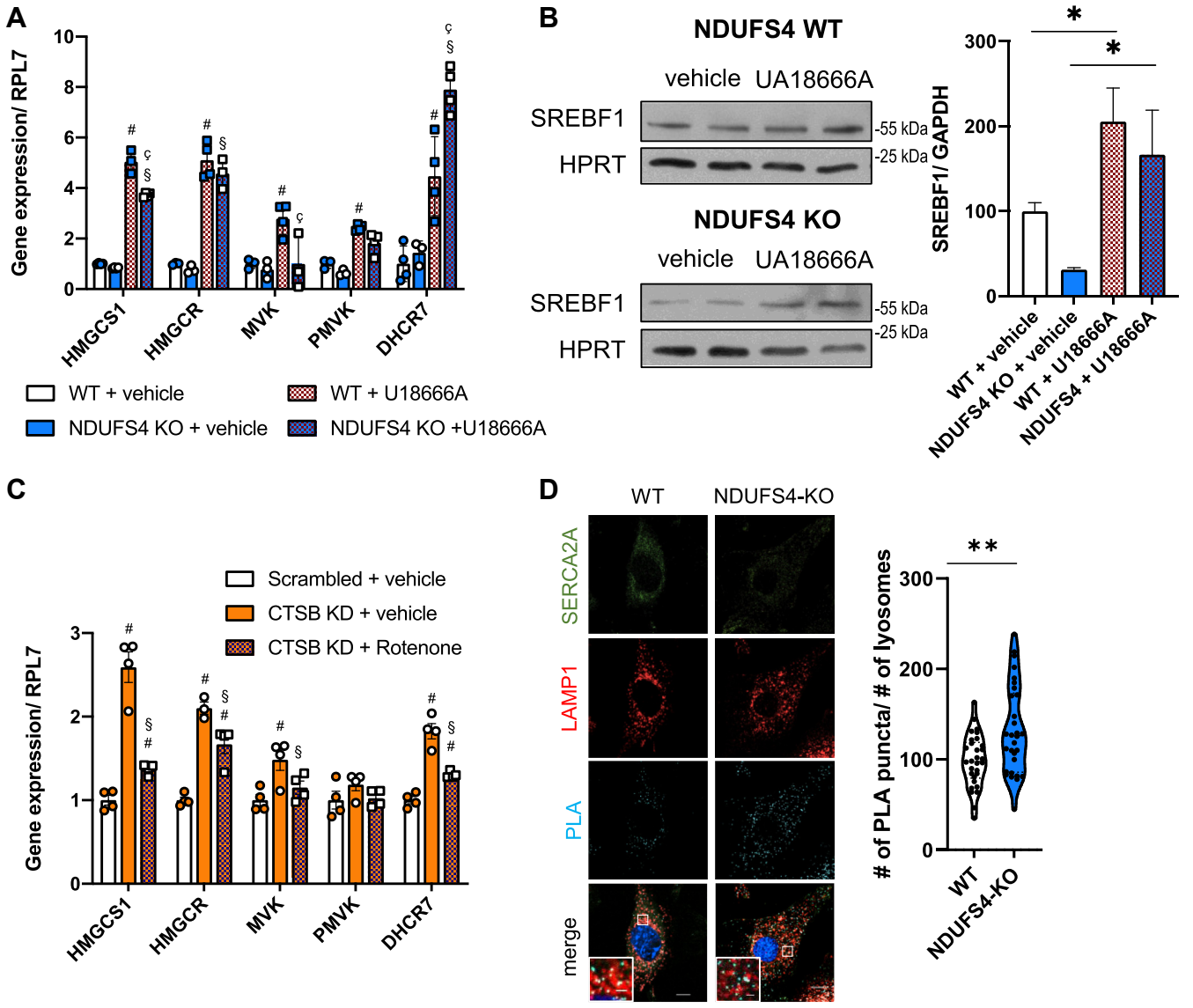

Figure 5. The mechanisms of cholesterol trafficking and homeostasis are fully functional in RC-deficient cells. *A*, qPCR showing the transcript level of cholesterol synthesis enzymes in WT and NDUFS4 KO MEF cells untreated and treated with the NPC1 inhibitor U18666A (4 h, 10 μM). At least three independent samples were evaluated for the experiments. Two-way ANOVA with Tukey's multiple comparisons test was used to determine the statistical significance. # = significant difference from control, § = significant difference from NDUFS4 KO, Ç = significant difference from control + U18666A. *B*, Western blot analysis showing SREBF1 level in WT and NDUFS4 KO MEFs untreated and treated with U18666A (4 h, 10 μM). HPRT was used as the loading control. *$p < 0.05$ *t* test, *C*, qPCR of genes involved in the cholesterol synthesis performed in control and CTSB KD HeLa cells untreated and treated with the mitochondrial complex I inhibitor Rotenone (250 nM, 24 h). The statistical significance was determined by two-way ANOVA with Tukey's multiple comparisons test, evaluating at least three independent samples, # = significant difference from control, § = significant difference from CTSB KD. *D*, representative confocal images showing the contact sites between the ER (detected by the marker SERCA2A) and lysosomes (marked with LAMP1) evaluated by proximity ligation (PLA) assay. *Right*: quantification of the number of PLA puncta counted on the area occupied by lysosomes. At least 30 cells were analyzed. The scale bar represents 10 μm; the scale bar on zoomed insets represents 2 μm. Statistical significance was evaluated using unpaired *t* test (**$p < 0.01$). CTSB, cathepsin B; ER, endoplasmic reticulum; MEF, mouse embryonic fibroblast; PLA, proximity ligation assay; qPCR, quantitative real-time PCR; RC, respiratory chain.

AMPK-DKO), and thus devoid of AMPK activity. It is noteworthy that AMPK-DKO cells also show impaired lysosomal function, with lysosomal swelling, Ca^{2+} accumulation, and decreased lysosomal hydrolysis (7). The transcript levels of cholesterol synthesis enzymes are globally upregulated in AMPK-DKO cells (Fig. 6*A*). To test if these cells are able to dynamically respond to perturbations in cholesterol homeostasis, we treated them with the NPC1 inhibitor U18666A (10 μM, 24 h). We observed an increase in the expression of cholesterol synthesis enzymes both in WT and AMPK-DKO cells (Fig. S4*A*). The levels of mature SREBF1 are increased in DKO cells, in agreement with the higher transcript levels of SREBF1 targets (Fig. 6*B*). No change was observed in AMPK activation in WT cells treated with U18666A (Fig. S4*B*). Therefore, lower AMPK activity cannot explain the decrease in the transcript levels of cholesterol synthesis enzymes observed in RC-deficient cells and tissues. Furthermore, reactivation of AMPK in UQCRC1-kd cells was not sufficient to restore the transcript levels of cholesterol synthesis enzymes to control levels (Fig. S4*C*).

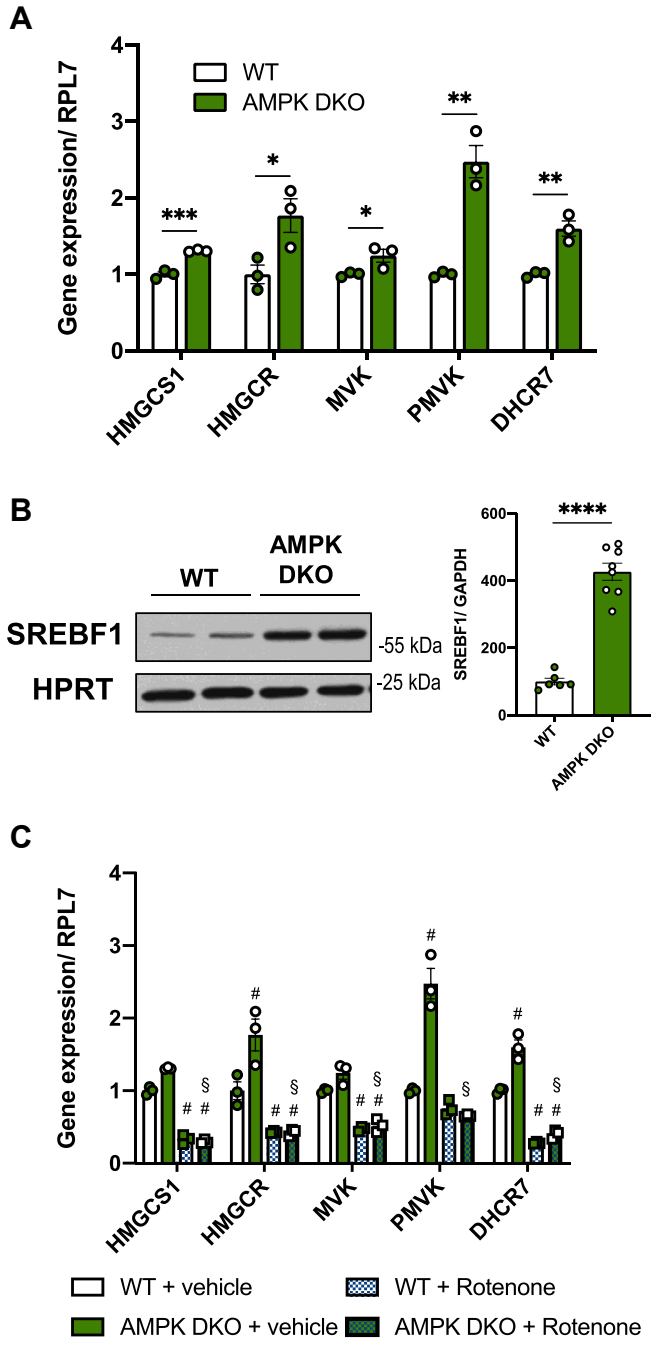

Figure 6. Downregulation of cholesterol synthesis in cells with mitochondrial dysfunction is independent of AMPK. *A*, qPCR of cholesterol synthesis genes in control and AMPK DKO MEFs. Three independent samples were evaluated. Statistical significance between control and mutant samples for each gene was determined by unpaired *t* test, $*p < 0.05$, $**p < 0.01$, $***p < 0.001$. *B*, Western blot analysis showing the level of SREBF1 in WT and AMPK DKO MEFs. At least six independent samples were analyzed using unpaired *t* test, $****p < 0.0001$. *C*, qPCR performed in WT and AMPK DKO MEFs untreated and treated with Rotenone. Three independent samples were evaluated. The statistical analysis was carried on using the two-way ANOVA with Tukey's multiple comparisons test, # = significant difference from control, § = significant difference from AMPK DKO. AMPK, AMP-activated protein kinase; DKO, double knockout; MEF, mouse embryonic fibroblast; qPCR, quantitative real-time PCR.

To verify that the response of cholesterol synthesis regulation to acute inhibition of the RC was independent of AMPK, we treated AMPK-WT and AMPK-DKO cells with the RC complex I inhibitor rotenone. We observed a global downregulation of the transcripts of cholesterol synthesis enzymes both in WT and AMPK-DKO cells (Fig. 6*C*).

AMPK and mTORC1 cross-regulate each other. Additionally, mTORC1 regulates cholesterol synthesis and has previously been shown to be hyperactive in the brain of NDUFS4-KO mice (12). To test if mTORC1 was involved in the transcriptional regulation of cholesterol synthesis in RC-deficient cells, we treated NDUFS4-KO cells with torin, an established inhibitor of mTORC1 (46). While torin treatment effectively blocked mTORC1 activity in both WT and NDUFS4-KO cells (Fig. S4*D*) and lowered the transcript levels of cholesterol enzymes in WT cells (Fig. S4*E*), there was no effect of mTORC1 inhibition on the transcript levels of cholesterol enzymes in NDUFS4-KO cells (Fig. S4*E*). These results suggest that mTORC1 is not involved in the downregulation of cholesterol synthesis enzyme transcript levels in NDUFS4-KO cells.

MCOLN1 loss-of-function decreases cholesterol synthesis in cells with mitochondrial defects

The observation that mitochondrial defects result in decreased expression of cholesterol synthesis enzymes, whereas lysosomal defects have the opposite effect, implies that the changes in the expression of the cholesterol pathway in mitochondrial defects cannot be explained simply by decreased lysosomal hydrolysis, as demonstrated above. Furthermore, changes in AMPK and mTORC1 activity also cannot explain this differential effect. We have previously shown that in cells with RC deficiencies, such as HeLa UQCRC1-kd and NDUFS4-KO mouse fibroblasts, there is decreased activity of TRPML1 (also known as mucolipin 1, MCOLN1). TRPML1 is a lysosomal export channel for divalent cations particularly implicated in lysosomal Ca^{2+} efflux (47). Thus, we tested if loss of MCOLN1 activity impacts the expression of cholesterol synthesis enzymes. We used mouse fibroblasts lacking MCOLN1 (MCOLN1-KO) and the corresponding WT cells, and measured the transcript levels of cholesterol synthesis enzymes by qPCR. We observed that the transcript levels of the cholesterol synthesis enzymes were downregulated in MCOLN1-KO (Fig. 7*A*). This result is similar to what is observed in cells with mitochondrial defects. This suggests that the loss of MCOLN1 activity, and corresponding accumulation of Ca^{2+} and possibly other divalent ions in the lysosome, correlates with the repression of the cholesterol synthesis pathway. To further demonstrate that the decrease in MCOLN1 activity was causative of the decreased transcript levels of the cholesterol synthesis enzymes, we tested if reactivating the MCOLN1 channel in RC-deficient cells would affect the expression of cholesterol synthesis enzymes. We treated the NDUFS4-KO cells with the MCOLN1 activator MLSA1, and observed an increase in the transcript levels of cholesterol synthesis enzymes (Fig. 7*B*). We obtained a similar result when treating UQCRC1-kd cells with MLSA1 (Fig. 7*C*), suggesting that lower MCOLN1 activity in cells with RC defects is a key mediator of cholesterol synthesis

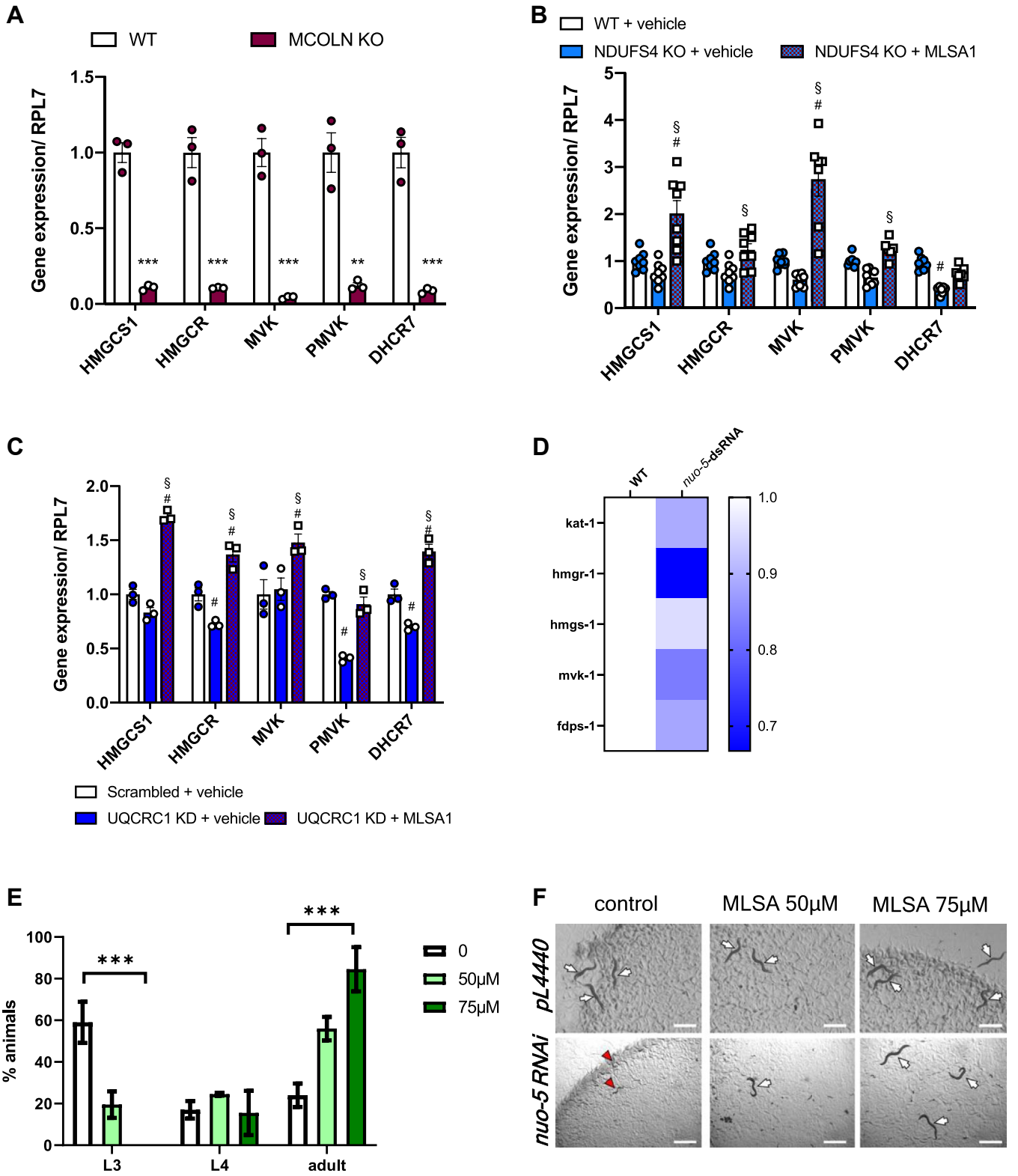

Figure 7. MCOLN1 loss-of-function decreases cholesterol synthesis in cells with mitochondrial deficiency and improves an *in vivo* model of mitochondrial disease. *A*, qPCR of genes involved in the cholesterol biosynthesis pathway in WT and MCLN KO MEFs. Three independent samples were evaluated. The statistical significance was determined by two-way ANOVA with Tukey's multiple comparisons test. $^{**}p < 0.01$, $^{***}p < 0.001$. The same genes were analyzed through qPCR in WT and NDUFS4 KO MEFs untreated and treated with the MCOLN1 activator MLSA1 (*B*). At least four independent replicates were evaluated. Statistical significance was evaluated with two-way ANOVA with Tukey's multiple comparisons test. # = significant difference from control, § = significant difference from NDUFS4 KO. qPCR of these genes was also performed in control and UQCRC1 KD HeLa cells, untreated and treated with MLSA1 (*C*). Three independent samples were used and analyzed using two-way ANOVA with Tukey's multiple comparisons test. # = significant difference from scrambled, § = significant difference from UQCRC1 KD. *D*, heatmap showing the fold change in the transcript levels of the indicated genes in *nuo-5* worms relative to their parental control line. *E*, percentage of *nuo-5*-dsRNA worms in larval 3 (L3), larval 4 (L4) and adult stages, in regular NGM in the absence or presence of MLSA1 (50 µM or 75 µM). After 4 days, from eggs laid from WT animals fed bacteria transformed either with empty vector (pl4440)

repression. These results highlight that MCOLN1 activity impacts the regulation of cholesterol homeostasis, akin to other roles played by this protein in nutrient sensing (48).

To test if activation of MCOLN1 might have benefits *in vivo*, we used a *Caenorhabditis elegans* model of mitochondrial RC deficiency with a silenced complex I subunit *nuo*-5 (an ortholog of mammalian complex I subunit NDUFS1), which we previously characterized (49). The *nuo-5*-dsRNA worms show larval arrest primarily in the L3 stages, and a delay in reaching adulthood (only about 25% of *nuo-5*-dsRNA worms reach adulthood on day 4, compared to 100% of WT worms who reach adulthood on day 3) (49). While *C. elegans* do not synthesize cholesterol, the mammalian cholesterol pathway is conserved in worms until the synthesis of mevalonate (50). Of note, because worms lack the ability to synthesize cholesterol from mevalonate, they rely on exogenous cholesterol, and decrease in cholesterol availability in the diet results, similar to mitochondrial deficiency in developmental arrest (51). It is thus possible that the decrease in the expression of mevalonate synthesis enzymes in *nuo-5*-depleted worms contributes to lower availability of mevalonate and to the developmental delay. In support of this possibility, we used a transcriptome dataset of *nuo-5*-dsRNA worms that we previously published (49) to assess the expression of mevalonate synthesis enzymes, and observed a global downregulation across the pathway (Fig. 7*D*; the transcripts for PMVK, MVD, and IDI1 were not detected in the dataset). Interestingly, we previously identified an acetylcholine signaling defect in the *C. elegans* mitochondrial disease model (49), a cellular function which is tightly linked to cholesterol homeostasis (52). Given the results obtained in cell lines with reactivation of the lysosomal channel MCOLN1, we thus sought to test if treating the worms with MLSA1 would be beneficial. We titrated addition of MLSA1 to the culture medium of *nuo-5*-dsRNA, in two different doses (50 μM and 75 μM) and observed that the percentage of worms reaching adulthood by day 4 increased proportionally to the concentration of MLSA1 (Fig. 7, *E* and *F*). While the consequences of MLSA1-induced MCOLN1 reactivation likely go beyond the effect on the expression of cholesterol/mevalonate synthesis enzymes, these results show that the pathological consequences triggered by defects in the RC can be, at least in part, rescued by manipulating the lysosome. This manipulation, among other pathways, will improve cholesterol homeostasis.

Discussion

Here, we demonstrate that the transcriptional regulation of the cholesterol synthesis pathway is impacted by both mitochondrial and lysosomal defects in an opposing manner. These data are supported by whole cell transcriptome data from cells with various mitochondrial and lysosomal defects, as well as tissues from murine models of mitochondrial or lysosomal defects and a nematode model of mitochondrial disease.

Cholesterol is an important constituent of cellular membranes; therefore, its expression levels are subject to a complex regulatory network that involves multiple cellular organelles and proteins. This network allows regulation of cholesterol synthesis at both transcriptional and posttranslational levels. At the transcriptional level, the regulation of cholesterol synthesis relies on the SREBPs transcription factors, of which SREBF1-a and SREBF2 are the predominant isoforms in cultured (mammalian) cell lines (37). Here, we observed an increase in the transcript levels of cholesterol synthesis enzymes in multiple cell models with different lysosomal defects, as well as in mouse models of lysosomal deficiency. Conversely, in cellular and mouse models of mitochondrial RC deficiency, we observed a decrease in the transcript levels of cholesterol synthesis enzymes. We also observed a decrease in the transcript levels of mevalonate synthesis enzymes in worms silenced for *nuo-5*, a subunit of RC complex I, indicating that this effect is also conserved in nematodes. While SREBF1 is usually seen as a generic activator of lipid synthesis and SREBF2 a more specific activator of the cholesterol synthesis pathway (53), here we observed that, in the cellular models of mitochondrial or lysosomal defects, the changes in the transcript levels of the cholesterol synthesis enzymes were paralleled by changes in SREBF1 protein levels and intracellular localization, while SREBF2 levels remained unchanged. In cellular models of lysosomal defects, SREBF1 was more abundant in the nucleus, in agreement with the increased transcript levels of the cholesterol synthesis enzymes. In cells with mitochondrial RC defects, there was less SREBF1 protein, and lower transcript levels of the same enzymes. As the transcript levels of SREBF1 were unchanged in the cells with lysosomal or mitochondrial defects, the decrease of SREBF1 protein levels in cells with mitochondrial defects could be due to proteolytic degradation. Interestingly, we observed that the decrease in SREBF1 protein levels could be prevented by inhibition of the proteasome, supporting the notion that SREBF1 was being actively targeted for degradation in the cellular models of RC deficiency. It has been previously described that SREBF1 can be subjected to ubiquitin-mediated proteolysis, and that the phosphorylation of SREBF1 by GSK3B promotes this process (38). Accordingly, we found that GSK3B was hyperactive in the cellular models of RC deficiency, providing a means to explain why SREBF1 levels were decreased in those cells. Activation of GSK3B has been reported in cells with 1-methyl-4-phenylpyridinium iodide (MPP(+))-induced mitochondrial malfunction (54). A study of urinary stem cells from patients of mitochondrial encephalopathy, lactic acidosis, and stroke-like episodes shows a decrease in GSK3B phosphorylation, which would correlate with increased activity, but the total levels of GSK3B were not measured, and therefore it is not clear if the protein is indeed active (55). In contrast, human

or with dsRNA against *Caenorhabditis elegans* complex I subunit NDUFS1 (*nuo-5*). ***$p < 0.0001$ two-way ANOVA. *F*, representative pictures of *C. elegans* treated either with pL4440 (empty vector) or with RNAi against nuo-5, after 4 days from egg-lay. *Arrows* (*white*) mark not arrested, developed into adulthood nematodes while arrowheads (*red*) mark arrested larvae. The scale bars represent 500 μm. MCOLN1, mucolipin 1; MEF, mouse embryonic fibroblast; NGM, nematode growth media; qPCR, quantitative real-time PCR.

fibroblasts with mutations in NPC1, which result in lysosomal cholesterol storage, show an increase in the inhibitory phosphorylation on GSK3B, and therefore decreased GSK3B activity (56). While this result needs to be tested in a more systematic manner, it is possible that the differential activation of GSK3B by mitochondrial and lysosomal defects contributes to the opposite regulation exerted over the transcription of genes encoding cholesterol synthesis enzymes. The mechanism that regulates GSK3b in response to defects in mitochondria or in lysosomes warrants further investigation. It is also possible that, in addition to cholesterol, other lipids are affected, given the lipogenic role of SREBF1.

The upregulation of cholesterol synthesis at transcript level by different lysosomal defects has been shown. Some of these defects include absence or loss-of-function of the proteins NPC1 and NPC2, which are involved in the lysosomal egress of cholesterol and sphingomyelin (19). Other lysosomal defects or interventions that impact acidification also result in transcriptional activation of cholesterol synthesis (27, 57, 58). The models of lysosomal defects that we assessed are KO of four different lysosomal genes: GAA, involved in lysosomal glycogen hydrolysis (59), cathepsins B and L, which are involved in lysosomal proteolysis (60), and LAMP2, involved in chaperone-mediated autophagy and cholesterol trafficking (61). All these mouse fibroblasts with different lysosomal defects yielded similar consequences to the transcriptional regulation of cholesterol synthesis. These results were also similar to those we obtained in HeLa cells with lysosomal defects, indicating that this effect is likely valid across cell types. Furthermore, we obtained similar results from the brain and liver of the mouse models studied, indicating a conserved effect across tissues. It is important to note that the transcriptional regulation of cholesterol synthesis in the liver is not only dependent on SREBPs but also nuclear receptors such as liver X receptors (LXRs) may also be involved (62).

The lysosomes are intracellular logistics platforms, processing and sensing several nutrients and distributing them to other cellular regions. They communicate with other organelles such as the ER and mitochondria. It is known that perturbation of lysosomal contact sites with the ER results in lysosomal cholesterol storage and increased association between the lysosomes and mitochondria (43). In the cellular model of RC deficiency, we did not observe any difference in the number of mitochondria-lysosome contact sites, but the contacts between the lysosomes and the ER were increased, which may facilitate transfer of cholesterol between the ER and the lysosomes. Cholesterol transfer at ER-lysosome contact sites can occur in both directions (63), but given that there is less SREBF1 in the models of mitochondrial malfunction, it is unlikely that there is net transfer of cholesterol from ER to lysosomes in these cells. The contribution of ER-lysosome-mitochondria cholesterol transfer through contact sites to the transcriptional regulation of cholesterol in models of mitochondrial and lysosomal malfunction remains to be determined.

We show here that the effect of lysosomal malfunction on cholesterol synthesis requires a functional RC. When we perturb mitochondrial respiration in cellular models of lysosomal deficiency, the transcriptional upregulation of cholesterol synthesis subsides. This observation raises tantalizing possibilities of targeting the RC to lower cholesterol synthesis in models of hypercholesterolemia. For example, metformin, a RC complex I inhibitor that is widely used as a drug against type II diabetes, reduces serum cholesterol levels in patients (64, 65). Cells treated with metformin also show a transcriptional downregulation of cholesterol synthesis (66, 67), although this may involve metformin-induced AMPK activation (68). In our cellular models of mitochondrial malfunction, we did not observe a role for AMPK or mTORC1 in the transcriptional regulation of cholesterol synthesis. Notably, acute pharmacological inhibition of different RC complexes appears to have an inhibitory effect on the transcription of cholesterol synthesis enzymes in cells (69, 70).

We showed previously that lysosomes accumulate Ca^{2+} in models of mitochondrial RC deficiency, due to decreased activity of the lysosomal Ca2+-export channel MCOLN1 (7). Interestingly, we observed that treatment of RC-deficient cells with an MCOLN1 agonist normalized the transcript levels of cholesterol synthesis enzymes. Furthermore, we observed that pharmacological activation of MCOLN1 significantly rescued the developmental delay that characterizes the worms silenced for *nuo-5*, a model of mitochondrial RC deficiency, suggesting that the normalization of cholesterol homeostasis contributed to the systemic improvement in the *nuo-5*-treated worms. Notably, upregulation of cholesterol synthesis in complex I-deficient mice improves their motor function and survival (71). Future studies will further detail the mechanisms by which mitochondrial and lysosomal defects impact the transcriptional regulation of cholesterol synthesis and the pathophysiological impacts of this process.

Experimental procedures

Cell culture and treatments

Perinatal mouse fibroblasts were cultured in Dulbecco's modified Eagle's medium (Gibco) supplemented with 10% v/v fetal bovine serum and 1% Penicillin/Streptomycin (Corning). Cell lines were maintained at 37 °C in a 5% CO2 controlled atmosphere. TrypLE (Gibco) was used to detach cells and generate subcultures. When at 80% of confluency, cells were treated with, MG132 (10 μM, 2 h), U18666A (10 μM, 24 h), with MLSA1 (20 μM, 4 h). The NDUFS4-KO cells and the GAA-KO cells were obtained as previously described (7, 20). The CTSB-KO, CTSL-KO mouse embryonic fibroblasts were a kind gift from Prof Thomas Reinheckel (Albert-Ludwigs-Universität Freiburg, Germany). The LAMP2-KO mouse embryonic fibroblasts were a kind gift from Prof Paul Saftig (University of KielGermany). The AMPKα1α2-DKO mouse embryonic fibroblasts were a kind gift from Prof Benoit Violet (Institut Cochin, Paris).

Generation of stable knockdown cells

Lentiviral stable knockdown generation was done by growing HEK293T packaging cells in Dulbecco's modified

Eagle's medium high glucose supplemented with 10% fetal bovine serum. After 24 h they were transfected with viral components and shRNA against target genes (or scrambled control) using Lipofectamine 2000 (Invitrogen, 11668-019), grown and concentrated using Lenti-X Concentrator (Clontech Laboratory, 631232) according to the manufacturer's instructions. The shRNA constructs were purchased from Open Biosystems (Dharmacon). HeLa cells were then seeded at 12,000 cells/cm2 and grown overnight to 70 to 80% confluence. These cells were transduced with the lentiviral particles using Polybrene (8 μg/ml; Sigma-Aldrich TR-1003-G). Puromycin (Thermo Fisher Scientific, BP2956-100; 4 μg/ml) was used as selection agent. These knocked down cells were selected with puromycin, the resistance marker of the shRNA vector, and stable silenced lines were established (Fig. S1).

RNA sequencing

RNA sequencing was performed as described (72). RNAseq data analysis was performed using Partek Software (https://www.partek.com/) Suite. RNAseq data were aligned to the reference genome mm10 by the BowTie algorithm, and the transcripts were quantified using the "mm10-Ensembl Transcripts release 95" as reference. For differential expression analysis, Bonferroni multitest correction was applied, and adjusted p-value<0.05 was considered significant. Ingenuity Pathway Analysis was used for assessment of transcription factor activity, as described (27). The data are deposited at Gene Expression Omnibus (GSE256471).

Mouse tissues

The NDUFS4-KO and GAA-KO mouse tissues were obtained as described earlier (Lorena Autophagy, King eLife1, eLife2). All animal experiments were carried out in accordance with the European guidelines for animal welfare and were approved by the Lower Saxony Landesamt fur Verbraucherschutz and Lebensmittelsicherheit (LAVES) registration number 15-883.

C. elegans *strains and maintenance*

We use standard nematode culture conditions. All strains were maintained at 20 °C on nematode growth media agar supplemented with *Escherichia coli* (OP50 or transformed HT115), unless otherwise indicated. The dsRNA transformed bacteria for feeding were derived from the Ahringer *C. elegans* RNAi library (52): nuo-5 (Y45G12B.1). Worm pictures were acquired with a Leica MZ10F modular stereo microscope connected to a digital camera.

Development assay and treatment with MLSA1

Both dsRNA bacterial clones (sequence validated), were grown in LB media to a concentration of 0.9 absorbance and spotted on nematode growth media plates. Prior the addition of MLSA1, dried bacteria were inactivated by UV light exposure for 25 min. Afterward, the compound dissolved in dimethyl sulfoxide was spotted at the desired final concentration (namely 50 μM and 75 μM). Plates were allowed to dry overnight at room temperature (RT) and subsequently stored at 4 °C. The first generation of nematodes (P0) was grown on RNAi plates without the compound. The second generation (F1) was grown on the MLSA1-supplemented plates. The developmental stage of the F1 was checked on the second, third, and fourth day after egg-lay. The percentage of animals in each developmental stage was calculated at each time point, and the data were pooled from two independent experiments.

Cell lysis and immunoblotting

Cells were harvested in lysis buffer (N-dodecyl maltoside (Dot Scientific) 1.5% w/v dissolved in PBS supplemented with protease and phosphatase inhibitor cocktail (Thermo Fisher Scientific). Lysates were incubated on ice for 30 min and cleared by centrifugation at 16,000*g* for 30 min at 4 °C. Supernatants were collected and stored at −20 °C until used. Protein concentration in the samples was evaluated using the Pierce BCA Protein Assay Kit (Thermo Fisher Scientific) following the manufacturer's instructions. A total of 50 μg of protein lysates was boiled for 10 min at 100 °C and loaded 13% Tris-glycine polyacrylamide gels in SDS/Tris-glycine running buffer. PageRuler plus prestained protein ladder (Thermo Fisher Scientific) were used for protein size estimation. The resolved proteins were transferred onto nitrocellulose membranes (Amersham) through a *Trans*-Blot semi-dry transfer cell (Bio-Rad). Membranes were subsequently blocked in Tris-buffered saline plus 0.1% Tween (TBS-T) plus 5% nonfat milk for 1 h at RT and then incubated over-night at 4 °C with primary antibodies diluted in TBS-T plus 5% nonfat milk. Membranes were then washed in TBS-T (3 × 10 min) at RT and subsequently incubated for 1 h at RT with horseradish peroxidase-conjugated secondary antibodies. Membranes were then washed in TBS-T (3 × 10 min) at RT and rinsed in TBS-T. Immunoreactive proteins were visualized using Immobilon Forte Western HRP Substrate (Merck Millipore) at the Imager Fluor-Chem M (Proteinsimple). Densitometric analysis was carried out using the Image J software (https://imagej.net/software/fiji/).

The following antibodies were used for Western blotting: mouse SREBP1 (Abcam AB3259), mouse SREBP2 (RD system MAB7119), mouse GAPDH (Sigma-Aldrich G8795) rabbit HPRT (Abcam, AB10479), rabbit Insig1 (Abcam,AB70784), rabbit SCPAP (Abcam, AB153933), rabbit PARP (Cell Signaling Technology, 542S), rabbit GSK3-beta (Cell Signaling Technology D5C5Z), rabbit SGK3-alpha/beta phosphor S21/S9 (Cell Signaling Technology, D8SeE12), PDI (Cell Signaling Technology, C81H6).

Cell fractionation

Cell fractionation of nuclear and cytoplasmic compartments was performed with the NE-PER Nuclear and Cytoplasmic Extraction Reagents (Thermo Fisher Scientific) kit following the manufacturer's instructions.

To obtain ER fractions, NDUFS4 WT and KO MEF cells grown on 15-cm dishes were resuspended in 10 mM NaCl,

1.5 mM MgCl2, 10 mM and Tris–HCl, pH 7.5 buffer and homogenized using an overhead stirrer (Wheaton instruments) with a Teflon pestle. Following homogenization, cells were subjected to differential centrifugation to obtain nuclear, whole cell, crude mitochondria and microsomal fractions. The latter were ultracentrifuged at 100 000*g* for 1 h to isolate ER fractions.

Immunocytochemistry, PLA and confocal imaging

Cells were cultured onto 12 mm glass coverslips (Thermo Fisher Scientific) coated with Poly-L-Lysine (Sigma-Aldrich). Cells were fixed with 4% w/v paraformaldehyde for 1 h at RT. After cell permeabilization in PBS plus Triton 0.1% for 30 min at RT and a blocking step performed in 3% bovine serum albumin dissolved in PBS for 30 min at RT, cells were stained with the appropriate primary antibodies diluted in PBS plus 3% bovine serum albumin overnight at 4 °C. Subsequently, for immunostaining experiments cells were washed three times in PBS and incubated with the secondary antibody Alexa Fluor 488 conjugated (Invitrogen) or Alexa Fluor 568 conjugated (Invitrogen). To perform the PLA assay the Duolink *In Situ* Detection reagents (Sigma-Aldrich) were used. Briefly, after primary antibodies staining, cells were incubated for 1 h at 37 °C with PLUS and MINUS PLA probes (Sigma-Aldrich). Then cells were incubated with the ligase diluted in the ligation buffer for 30 min at 37 °C; subsequently, the amplification step was performed by incubating cells with the polymerase diluted in the amplification buffer for 1 h at 37 °C. Cells were finally incubated with Hoechst 33258 (Invitrogen) for 5 min at RT and mounted with the ProLong Diamond Antifade (Invitrogen) mounting medium on glass slides.

Images were acquired with a LeicaSP7 confocal microscope (Leica Microsystems) and quantified using ImageJ.

The following antibodies were used: mouse SERCA 2ATPase (Invitrogen MA3-919), mouse HSP60, rabbit LAMP1 (Cell Signaling Technology, C54H11), mouse HSP60 (Proteintech 66041-1)

Real-time qPCR

RNA was extracted from MEF cells using the RNeasy Mini Kit (Qiagen) following manufacturer's instructions. RNA quality and concentration were assessed by Nanodrop. Complementary DNA (cDNA) was synthesized from total RNA using iScript cDNA Synthesis Kit (Bio Rad). A total of 100 ng cDNA has been used for each qPCR reaction. qPCR reactions were performed on 98-well plate adding to the cDNA the PowerUp SYBR Green Master Mix (Applied Biosystems) and the DNA primers.

The following primers were used:

DHCR7. For: AGGCTGGATCTCAAGGACAAT. Rev: GCCAGACTAGCATGGCCTG.

HMGCR. For: TGTTCACCGGCAACAACAAGA. Rev: CCG CGTTATCGTCAGGATGA.

HMGCS1. For: CGGATCGTGAAGACATCAACTC. Rev: CGCCCAATGCAATCATAGGAA.

MVK. For: GGTGTGGTCGGAACTTCCC. Rev: CCTT GAGCGGGTTGGAGAC.

PMVK. For: AAAATCCGGGAAGGACTTCGT. Rev: AGAGCACAGATGTTACCTCCA.

TULP3. For: CAGTGCCTTTGACGATGAGAC. Rev: TTC TGGGTTTGGCTGTACCAT.

PLEKF1. For: GAGAGCTGTTTTGGGGCATC. Rev: AATACTGCCGTACACCAGGAT.

IL20RB. For: ACCCCTTTAACCGAAATGCAA. Rev: CCTCCAGTAGACCACAAGGAA.

SH3RF1. For: CAGGTCCATATAAGCACCACTG. Rev: GG TAGGGGACATCTGAAGGGA.

NUCB2. For: GGACAAGACCAAAGTACACAACA. Rev: CCGCTCCTTATCTCCTCTATGT.

SDF2L1. For: CTGCACTCACACGACATCAAA. Rev: CGCGAATCCGCCAGTAACT.

SCAP: For: CCGAGCATTCCAACTGGTG. Rev: CCAT GTTCGGGAAGTAGGCT.

SREBP1: For:TGACCCGGCTATTCCCTGA. Rev: CTGGGCTGAGCAATACAGTTC.

SREBP2: For: GCAGCAACGGGACCATTC. Rev:CCCCATGACTAAGTCCTTCAACT.

RPL7. For: CTGCTGGGCCAAAAACTCTCA. Rev: CCTTCAACTCTGCGAAATTCCTT.

Cholesterol assay

The amount of cholesterol in the cell ER fractions was evaluated through Amplex cholesterol Assay kit (Invitrogen A12216) following the manufacturer's instructions.

Data availability

The raw data from RNA sequencing are deposited at Gene Expression Omnibus (GSE256471). Other data are available upon reasonable request to the corresponding author.

Supporting information—This article contains supporting information.

Author contributions—F. A., L. P., J. D., K. F. Y., S. M., A. S., N. V., I. M., and N. R. writing–review and editing; F. A., L. P., J. D., K. F. Y., S. M., A. S., and N. R. investigation; F. A., K. F. Y., S. M., N. V., I. M., and N. R. formal analysis; F. A. and N. R. writing–original draft; L. P., I. M., and N. R. conceptualization; K. F. Y., S. M., N. V., I. M., and N. R. visualization; N. V., I. M., and N. R. funding acquisition; N. V., I. M., and N. R. supervision; N. V. and N. R. methodology; N. R. data curation; N. R. project administration; N. R. resources; N. R. validation.

Funding and additional information—The conclusion of this work was supported by the start-up funds from the Department of Cellular and Molecular Physiology at Penn State University and NIH R56AG082790-01 to N. R. and John Black Foundation and Wellcome Trust 224361/Z/21/Z to I. M. The initial stage of this work was supported by DAAD-Germany doctoral fellowship to L. P.; ERC Starting Grant 337327; DFG SFB1190-P02; FCT 2022.09311.PTDC; FCT PTDC/MED-NEU/8030/2020; La Caixa HR22-00854; German Research Foundation grants VE663/3-1 and

VE663/3-4 (N. V.). The content is solely the responsibility of the authors and does not necessarily represent the official views of the National Institutes of Health.

Conflict of interest—The authors declare that they have no conflicts of interest with the contents of this article.

Abbreviations—The abbreviations used are: AMPK, AMP-activated protein kinase; CTSB, cathepsin B; CTSL, cathepsin L; DEG, differentially expressed gene; DKO, double knockout; ER, endoplasmic reticulum; GAA, acid alpha-glucosidase; MCOLN1, mucolipin 1; MEF, mouse embryonic fibroblast; mTORC1, mechanistic target of rapamycin complex 1; PLA, proximity ligation assay; qPCR, quantitative real-time PCR; RC, respiratory chain; RT, room temperature; TBS-T, Tris-buffered saline plus 0.1% Tween.

References

1. Picard, M., and Shirihai, O. S. (2022) Mitochondrial signal transduction. *Cell Metab.* **34**, 1620–1653
2. Mottis, A., Herzig, S., and Auwerx, J. (2019) Mitocellular communication: shaping health and disease. *Science* **366**, 827–832
3. Viscomi, C., Bottani, E., Civiletto, G., Cerutti, R., Moggio, M., Fagiolari, G., *et al.* (2011) In vivo correction of COX deficiency by activation of the AMPK/PGC-1α axis. *Cell Metab.* **14**, 80–90
4. Dogan, S. A., Cerutti, R., Benincá, C., Brea-Calvo, G., Jacobs, H. T., Zeviani, M., *et al.* (2018) Perturbed redox signaling exacerbates a mitochondrial myopathy. *Cell Metab.* **28**, 764–775.e5
5. Toyama, E. Q., Herzig, S., Courchet, J., Lewis, T. L., Jr., Oliver, C., Hellberg, K., *et al.* (2016) AMP-activated protein kinase mediates mitochondrial fission in response to energy stress. *Science* **351**, 275–281
6. Raimundo, N., Song, L., Shutt, T. E., McKay, S. E., Cotney, J., Guan, M. X., *et al.* (2012) Mitochondrial stress engages E2F1 apoptotic signaling to cause deafness. *Cell* **148**, 716–726
7. Fernandez-Mosquera, L., Yambire, K. F., Couto, R., Pereyra, L., Pabis, K., Ponsford, A. H., *et al.* (2019) Mitochondrial respiratory chain deficiency inhibits lysosomal hydrolysis. *Autophagy* **15**, 1572–1591
8. Steinberg, G. R., and Hardie, D. G. (2023) New insights into activation and function of the AMPK. *Nat. Rev. Mol. Cell Biol.* **24**, 255–272
9. Napolitano, G., Di Malta, C., and Ballabio, A. (2022) Non-canonical mTORC1 signaling at the lysosome. *Trends Cell Biol.* **32**, 920–931
10. Lin, S. C., and Hardie, D. G. (2018) AMPK: sensing glucose as well as cellular energy status. *Cell Metab.* **27**, 299–313
11. Saxton, R. A., and Sabatini, D. M. (2017) mTOR signaling in growth, metabolism, and disease. *Cell* **168**, 960–976
12. Johnson, S. C., Yanos, M. E., Kayser, E., Quintana, A., Castanza, A., Uhde, L., *et al.* (2014) mTOR inhibition Alleviates mitochondrial disease in a mouse model of Leigh Syndrome. *Science* **342**, 1524–1528
13. Ito, T. K., Lu, C., Khan, J., Nguyen, Q., Huang, H. Z., Kim, D., *et al.* (2017) Hepatic S6K1 partially regulates lifespan of mice with mitochondrial complex I deficiency. *Front. Genet.* **8**, 1–8
14. Barriocanal-Casado, E., Hidalgo-Gutiérrez, A., Raimundo, N., González-García, P., Acuña-Castroviejo, D., Escames, G., *et al.* (2019) Rapamycin administration is not a valid therapeutic strategy for every case of mitochondrial disease. *EBioMedicine* **42**, 511–523
15. Carroll, B., and Dunlop, E. A. (2017) The lysosome: a crucial hub for AMPK and mTORC1 signalling. *Biochem. J.* **474**, 1453–1466
16. Fedele, A. O., and Proud, C. G. (2020) Chloroquine and bafilomycin A mimic lysosomal storage disorders and impair mTORC1 signalling. *Biosci. Rep.* **40**, 1–20
17. Castellano, B. M., Thelen, A. M., Moldavski, O., Feltes, M., Van Der Welle, R. E. N., Mydock-McGrane, L., *et al.* (2017) Lysosomal cholesterol activates mTORC1 via an SLC38A9-Niemann-Pick C1 signaling complex. *Science* **355**, 1306–1311
18. Lawrence, R. E., and Zoncu, R. (2019) The lysosome as a cellular centre for signalling, metabolism and quality control. *Nat. Cell Biol.* **21**, 133–142
19. Thelen, A. M., and Zoncu, R. (2017) Emerging roles for the lysosome in lipid metabolism. *Trends Cell Biol.* **27**, 833–850
20. Yambire, K. F., Rostosky, C., Watanabe, T., Pacheu-Grau, D., Torres-Odio, S., Sanchez-Guerrero, A., *et al.* (2019) Impaired lysosomal acidification triggers iron deficiency and inflammation in vivo. *Elife* **8**, 1–36
21. Weber, R. A., Yen, F. S., Nicholson, S. P. V., Alwaseem, H., Bayraktar, E. C., Alam, M., *et al.* (2020) Maintaining iron homeostasis is the key role of lysosomal acidity for cell Proliferation. *Mol. Cell* **77**, 645–655.e7
22. Miles, A. L., Burr, S. P., Grice, G. L., and Nathan, J. A. (2017) The vacuolar-ATPase complex and assembly factors, TMEM199 and CCDC115, control HIF1α prolyl hydroxylation by regulating cellular Iron levels. *Elife* **6**, 1–28
23. Deus, C. M., Yambire, K. F., Oliveira, P. J., and Raimundo, N. (2020) Mitochondria–lysosome crosstalk: from physiology to neurodegeneration. *Trends Mol. Med.* **26**, 71–88
24. Wong, Y. C., Kim, S., Peng, W., and Krainc, D. (2019) Regulation and function of mitochondria–lysosome membrane contact sites in cellular homeostasis. *Trends Cell Biol.* **29**, 500–513
25. Baixauli, F., Acín-Pérez, R., Villarroya-Beltrí, C., Mazzeo, C., Nuñez-Andrade, N., Gabandé-Rodriguez, E., *et al.* (2015) Mitochondrial respiration controls lysosomal function during inflammatory t cell responses. *Cell Metab.* **22**, 485–498
26. Demers-Lamarche, J., Guillebaud, G., Tlili, M., Todkar, K., Bélanger, N., Grondin, M., *et al.* (2016) Loss of mitochondrial function impairs Lysosomes. *J. Biol. Chem.* **291**, 10263–10276
27. Yambire, K. F., Fernandez-mosquera, L., Steinfeld, R., Muhle, C., Ikonen, E., Milosevic, I., *et al.* (2019) Mitochondrial biogenesis is transcriptionally repressed in lysosomal lipid storage diseases. *Elife* **8**, 1–29
28. Li, T. Y., Wang, Q., Gao, A. W., Li, X., Sun, Y., Mottis, A., *et al.* (2023) Lysosomes mediate the mitochondrial UPR via mTORC1-dependent ATF4 phosphorylation. *Cell Discov.* **9**, 18–21
29. Li, T. Y., Gao, A. W., Li, X., Li, H., Liu, Y. J., Lalou, A., *et al.* (2023) V-ATPase/TORC1-mediated ATFS-1 translation directs mitochondrial UPR activation in C. elegans. *J. Cell Biol.* **222**, e202205045
30. Wong, Y. C., Ysselstein, D., and Krainc, D. (2018) Mitochondria-lysosome contacts regulate mitochondrial fission via RAB7 GTP hydrolysis. *Nature* **554**, 382–386
31. Wong, Y. C., Peng, W., and Krainc, D. (2019) Lysosomal regulation of Inter-mitochondrial contact fate and Motility in Charcot-Marie-Tooth type 2. *Dev. Cell* **50**, 339–354.e4
32. Peng, W., Wong, Y. C., and Krainc, D. (2020) Mitochondria-lysosome contacts regulate mitochondrial Ca2+ dynamics via lysosomal TRPML1. *Proc. Natl. Acad. Sci. U. S. A.* **117**, 19266–19275
33. Furuchi, T., Aikawa, K., Arai, H., and Inoue, K. (1993) Bafilomycin A1, a specific inhibitor of vacuolar-type H+-ATPase, blocks lysosomal cholesterol trafficking in macrophages. *J. Biol. Chem.* **268**, 27345–27348
34. Qian, H., Wu, X., Du, X., Yao, X., Zhao, X., Lee, J., *et al.* (2020) Structural Basis of Low-pH-dependent lysosomal cholesterol egress by NPC1 and NPC2. *Cell* **182**, 98–111.e18
35. Lim, J. A., Li, L., Kakhlon, O., Myerowitz, R., and Raben, N. (2015) Defects in calcium homeostasis and mitochondria can be reversed in Pompe disease. *Autophagy* **11**, 385–402
36. Chung, C., Puthanveetil, P., Ory, D. S., and Lieberman, A. P. (2016) Genetic and pharmacological evidence implicates cathepsins in Niemann-Pick C cerebellar degeneration. *Hum. Mol. Genet.* **25**, 1434–1446
37. Brown, M. S., Radhakrishnan, A., and Goldstein, J. L. (2018) Retrospective on Cholesterol homeostasis: the central role of scap. *Annu. Rev. Biochem.* **87**, 783–807
38. Punga, T., Bengoechea-Alonso, M. T., and Ericsson, J. (2006) Phosphorylation and ubiquitination of the transcription factor sterol regulatory element-binding protein-1 in response to DNA binding. *J. Biol. Chem.* **281**, 25278–25286
39. Trinh, M. N., Brown, M. S., Goldstein, J. L., Han, J., Vale, G., McDonald, J. G., *et al.* (2020) Last step in the path of LDL cholesterol from lysosome to plasma membrane to ER is governed by phosphatidylserine. *Proc. Natl. Acad. Sci. U. S. A.* **117**, 18521–18529
40. Infante, R. E., Radhakrishnan, A., Abi-Mosleh, L., Kinch, L. N., Wang, M. L., Grishin, N. V., *et al.* (2008) Purified NPC1 protein II. Localization of

sterol binding to a 240-amino acid soluble luminal loop. *J. Biol. Chem.* **283**, 1064–1075
41. Infante, R. E., Abi-Mosleh, L., Radhakrishnan, A., Dale, J. D., Brown, M. S., and Goldstein, J. L. (2008) Purified NPC1 protein: I. Binding of cholesterol and oxysterols to a 1278-amino acid membrane protein. *J. Biol. Chem.* **283**, 1052–1063
42. Infante, R. E., Wang, M. L., Radhakrishnan, A., Hyock, J. K., Brown, M. S., and Goldstein, J. L. (2008) NPC2 facilitates bidirectional transfer of cholesterol between NPC1 and lipid bilayers, a step in cholesterol egress from lysosomes. *Proc. Natl. Acad. Sci. U. S. A.* **105**, 15287–15292
43. Höglinger, D., Burgoyne, T., Sanchez-Heras, E., Hartwig, P., Colaco, A., Newton, J., *et al.* (2019) NPC1 regulates ER contacts with endocytic organelles to mediate cholesterol egress. *Nat. Commun.* **10**, 1–14
44. Scorrano, L., De Matteis, M. A., Emr, S., Giordano, F., Hajnóczky, G., Kornmann, B., *et al.* (2019) Coming together to define membrane contact sites. *Nat. Commun.* **10**, 1–11
45. Clarke, P. R., and Hardie, D. G. (1990) Regulation of HMG-CoA reductase: identification of the site phosphorylated by the AMP-activated protein kinase in vitro and in intact rat liver. *EMBO J.* **9**, 2439–2446
46. Thoreen, C. C., Kang, S. A., Chang, J. W., Liu, Q., Zhang, J., Gao, Y., *et al.* (2009) An ATP-competitive mammalian target of rapamycin inhibitor reveals rapamycin-resistant functions of mTORC1. *J. Biol. Chem.* **284**, 8023–8032
47. Di Paola, S., Scotto-Rosato, A., and Medina, D. L. (2018) TRPML1: the Ca(2+)retaker of the lysosome. *Cell Calcium* **69**, 112–121
48. Wang, W., Gao, Q., Yang, M., Zhang, X., Yu, L., Lawas, M., *et al.* (2015) Up-regulation of lysosomal TRPML1 channels is essential for lysosomal adaptation to nutrient starvation. *Proc. Natl. Acad. Sci. U. S. A.* **112**, E1373–E1381
49. Maglioni, S., Schiavi, A., Melcher, M., Brinkmann, V., Luo, Z., Laromaine, A., *et al.* (2022) Neuroligin-mediated neurodevelopmental defects are induced by mitochondrial dysfunction and prevented by lutein in C. elegans. *Nat. Commun.* **13**, 2620
50. Rauthan, M., and Pilon, M. (2011) The mevalonate pathway in C. Elegans. *Lipids Health Dis.* **10**, 1–12
51. Merris, M., Wadsworth, W. G., Khamrai, U., Bittman, R., Chitwood, D. J., and Lenard, J. (2003) Sterol effects and sites of sterol accumulation in Caenorhabditis elegans: developmental requirement for 4α-methyl sterols. *J. Lipid Res.* **44**, 172–181
52. Kamath, R. S., and Ahringer, J. (2003) Genome-wide RNAi screening in Caenorhabditis elegans. *Methods* **30**, 313–321
53. Shimano, H., and Sato, R. (2017) SREBP-regulated lipid metabolism: convergent physiology-divergent pathophysiology. *Nat. Rev. Endocrinol.* **13**, 710–730
54. Petit-Paitel, A., Brau, F., Cazareth, J., and Chabry, J. (2009) Involvment of cytosolic and mitochondrial GSK-3β in mitochondrial dysfunction and neuronal cell death of MPTP/MPP+-treated neurons. *PLoS One* **4**, e5491
55. Gao, X., Jiang, Z., Yan, X., Liu, J., Li, F., Liu, P., *et al.* (2021) ATF5, a putative therapeutic target for the mitochondrial DNA 3243A > G mutation-related disease. *Cell Death Dis.* **12**, 1–11
56. Wos, M., Komiażyk, M., Pikula, S., Tylki-Szymanska, A., and Bandorowicz-Pikula, J. (2019) Activation of mammalian terget of rapamycin kinase and glycogen synthase kinase-3β accompanies abnormal accumulation of cholesterol in fibroblasts from Niemann-Pick type C patients. *J. Cell. Biochem.* **120**, 6580–6588
57. Davis, O. B., Shin, H. R., Lim, C. Y., Wu, E. Y., Kukurugya, M., Maher, C. F., *et al.* (2021) NPC1-mTORC1 signaling Couples cholesterol sensing to organelle homeostasis and is a targetable pathway in Niemann-Pick type C. *Dev. Cell* **56**, 260–276.e7
58. Torres, S., Matías, N., Baulies, A., Nuñez, S., Alarcon-Vila, C., Martinez, L., *et al.* (2017) Mitochondrial GSH replenishment as a potential therapeutic approach for Niemann Pick type C disease. *Redox Biol.* **11**, 60–72
59. Fukuda, T., and Roberts, A. (2007) Acid alpha-glucosidase deficiency (Pompe Disease). *Curr. Neurol. Neurosci. Rep.* **7**, 71–77
60. Sevenich, L., Pennacchio, L. A., Peters, C., and Reinheckel, T. (2006) Human cathepsin L rescues the neurodegeneration and lethality in cathepsin B/L double-deficient mice. *Biol. Chem.* **387**, 885–891
61. Li, J., and Pfeffer, S. R. (2016) Lysosomal membrane glycoproteins bind cholesterol and contribute to lysosomal cholesterol export. *Elife* **5**, 1–16
62. Zelcer, N., and Tontonoz, P. (2006) Liver X receptors as integrators of metabolic and inflammatory signaling. *J. Clin. Invest.* **116**, 607–614
63. Lim, C. Y., Davis, O. B., Shin, H. R., Zhang, J., Berdan, C. A., Jiang, X., *et al.* (2019) ER–lysosome contacts enable cholesterol sensing by mTORC1 and drive aberrant growth signalling in Niemann–Pick type C. *Nat. Cell Biol.* **21**, 1206–1218
64. Pentikäinen, P. J., Voutilainen, E., Aro, A., Uusitupa, M., Penttilä, I., and Vapaatalo, H. (1990) Cholesterol lowering effect of metformin in combined hyperlipidemia: placebo controlled double blind trial. *Ann. Med.* **22**, 307–312
65. Fontbonne, A., Charles, M. A., Juhan-Vague, I., Andre, P., Isnard, F., Cohen, J.-M., *et al.* (1996) The effect of metformin on the metabolic abnormalities associated with upper-body fat distribution. BIGPRO Study Group. *Diabetes Care* **19**, 920–926
66. Bi, Y., Wu, W., Shi, J., Liang, H., Yin, W., Chen, Y., *et al.* (2014) Role for sterol regulatory element binding protein-1c activation in mediating skeletal muscle insulin resistance via repression of rat insulin receptor substrate-1 transcription. *Diabetologia* **57**, 592–602
67. Deng, J., Peng, M., Zhou, S., Xiao, D., Hu, X., Xu, S., *et al.* (2021) Metformin targets Clusterin to control lipogenesis and inhibit the growth of bladder cancer cells through SREBP-1c/FASN axis. *Signal Transduct. Target. Ther.* **6**, 2020–2022
68. Zhou, G., Myers, R., Li, Y., Chen, Y., Shen, X., Fenyk-Melody, J., *et al.* (2001) Role of AMP-activated protein kinase in mechanism of metformin action. *J. Clin. Invest.* **108**, 1167–1174
69. Wall, C. T. J., Lefebvre, G., Metairon, S., Descombes, P., Wiederkehr, A., and Santo-Domingo, J. (2022) Mitochondrial respiratory chain dysfunction alters ER sterol sensing and mevalonate pathway activity. *J. Biol. Chem.* **298**, 101652
70. Caria, I., Nunes, M. J., Ciraci, V., Carvalho, A. N., Ranito, C., Santos, S. G., *et al.* (2024) NPC1-like phenotype, with intracellular cholesterol accumulation and altered mTORC1 signaling in models of Parkinson's disease. *Biochim. Biophys. Acta Mol. Basis Dis.* **1870**, 166980
71. Schirris, T. J. J., Rossell, S., de Haas, R., Frambach, S. J. C. M., Hoogstraten, C. A., Renkema, G. H., *et al.* (2021) Stimulation of cholesterol biosynthesis in mitochondrial complex I-deficiency lowers reductive stress and improves motor function and survival in mice. *Biochim. Biophys. Acta Mol. Basis Dis.* **1867**, 166062
72. Murdoch, J. D., Rostosky, C. M., Gowrisankaran, S., Arora, A. S., Soukup, S. F., Vidal, R., *et al.* (2016) Endophilin-A deficiency Induces the Foxo3a-Fbxo32 network in the brain and causes Dysregulation of autophagy and the ubiquitin-proteasome system. *Cell Rep.* **17**, 1071–1086